Characterizing and Minimizing Sources of Error in Inertial Body Sensor Networks

Shanshan Chen, Jeff S. Brantley, Taeyoung Kim, Samuel A. Ridenour, John Lach*
Charles L. Brown Department of Electrical and Computer Engineering
University of Virginia
E-mail: {sc2xh,jb7fx,tk2np,sar7f,jlach}@virginia.edu
*Corresponding author

Abstract: Body sensor network (BSN) applications depend on accurate and precise data from body-worn devices, but issues related to sensor variations, body mounting variations, integration drift, and node-to-node synchronization can dramatically impact the quality and reliability of collected data and, ultimately, application fidelity. Characterizing and addressing these sources of error – which are both static and dynamic (e.g. sensors suffer from static manufacturing variability and dynamic environmental impacts) – within the context of application requirements is therefore necessary for the viability of such applications.

This work characterizes and addresses errors related to node synchronization, sensor and mounting calibration, and integration drift on a case study application – knee joint angle as measured during walking by the TEMPO 3.1 inertial BSN platform. Using the Vicon® optical motion capture system to provide ground truth, synchronization, calibration, and drift error are quantified, and the efficacy of solutions for reducing such errors is evaluated.

Keywords: Body sensor networks, calibration, integration drift, time synchronization

Biographical notes: Shanshan Chen received the M.S. (2008) in Telecommunication Engineering from the University of Oklahoma. She is currently pursuing the Ph.D. degree in Electrical Engineering at the University of Virginia. She has been awarded one US patent and has authored and co-authored several publications in the areas of network design and body sensor networks. Her general research interests include body sensor networks, inertial information retrieval and wireless health.

Jeff S. Brantley received the B.S. (2009) in Computer Engineering from Mississippi State University. He is currently pursuing the Ph.D. degree in Computer Engineering at the University of Virginia as an NSF Graduate Research Fellow. His research interests include embedded computing, resource-constrained signal processing, and body sensor networks for wireless health applications.

Taeyoung Kim received the B.S. (2005) in Electronics Engineering from the Konkuk University and a M.S. (2007) in Electronic and Computer Engineering from the Korea University. He is currently pursuing a Ph.D. in Electrical Engineering at the University of Virginia. His research interests include embedded networking systems, embedded computing, and body sensor networks. He is a student member of the IEEE.

Samuel A. Ridenour received the B.S. (2009) in Electrical Engineering and Computer Engineering from the University of Virginia, where he is currently pursuing the M.S. degree in Electrical Engineering. His research interests include embedded computing and signal processing, communications, and the medical application of body area sensor networks.

John Lach received the B.S. (1996) from Stanford University and the M.S. (1998) and Ph.D. (2000) in Electrical Engineering from UCLA. Since 2000, he has been on the faculty of the Charles L. Brown Department of Electrical and Computer Engineering at the University of Virginia and has held the rank of Associate Professor with tenure since 2006. His primary research interests are wireless health, wearable technologies for biomedical applications, integrated circuit design techniques, dynamically adaptable and real time embedded systems, fault and defect tolerance, safety-critical system design and analysis, general purpose and application specific processor design, and field programmable gate arrays (FPGAs). He has been the PI or co-PI on over 25 grants and has published over 85 refereed papers, including two Best Paper Awards. He is a Co-Founder and Steering Committee member for the Wireless Health conference series and a Technical Program Committee Co-Chair for BSN 2011. From 2005-2010, he was an Associate Editor for the IEEE Transactions on Computers and the IEEE Transactions on Computer Aided Design of Integrated Circuits and Systems. He is a Senior Member of the IEEE, and a member of the ACM, IEEE Computer Society, IEEE Circuits and Systems Society, IEEE VLSI Systems and Applications Technical Committee, ACM SIGDA, and Eta Kappa Nu. He is a Co-Founder and Co-Director of the UVA Center for Wireless Health.

1 Introduction

Inertial body sensor networks (BSNs) – wireless, body-worn nodes fitted with accelerometers and gyroscopes – have shown great promise for a number of application domains, but their utility ultimately depends on satisfying fidelity requirements (accuracy, precision, latency, reliability, etc.) specific to their target applications. A number of practical sources of error can affect the accuracy of inertial BSNs, and their effects must therefore be examined in the context of specific applications in order to determine their relative impacts on fidelity. Three critical sources of error across inertial BSN platforms and applications are those relating to synchronization, calibration, and drift. Synchronization errors become potentially critical for data fusion from a multi-node system measuring rapidly-changing, non-stationary signals. Calibration errors may occur not only at the sensor level, but also with respect to placement on the body due to body contour variations. Integration drift errors occur when converting from acceleration to velocity (or again to position displacement) or from rotational rate to angular displacement.

While these three types of errors are general across inertial BSN platforms, their impact on fidelity should be characterized in context in order to determine the relative importance of each source for a given application. To illustrate this, a case study is presented involving the measurement of knee joint angle, a common parameter in gait analysis, using the TEMPO 3.1 inertial BSN platform (Barth et al. (2009)), with a Vicon® optical motion capture system used to provide ground truth. The effect of synchronization, calibration, and drift errors on calculated joint angles is characterized, and methods for addressing and minimizing these errors are discussed and compared, including the time transmission synchronization approach used in TEMPO 3.1. While the error magnitude results are application-specific, the approach for error source characterization and minimization can be applied to any inertial BSN platform and target application.

The rest of this paper is organized as follows. Section 2 details the experimental setup for data collection and analysis. Sections 3 through 6 examine synchronization, sensor calibration, integration drift, and mounting calibration, respectively, and offer possible solutions for minimizing these errors within the knee joint angle measurement context. Each section presents experimental results showing a relative improvement over the results from the previous sections. Section 7 summarizes the overall analysis in the application context and concludes the paper.

2 Experimental Setup

To examine the impact of inertial BSN synchronization, calibration errors within an application context, a case study of knee joint angle measurement is presented. This application typically requires high accuracy but is quite sensitive to error sources.

2.1 Background

Among the many parameters in gait assessment, knee joint angle is of interest in several clinical research areas, such as osteoarthritis, orthopedics, prosthetics, and knee surgery recovery and rehabilitation. 3D position tracking motion analysis systems such as Vicon® have been developed as standard systems for measuring joint angles in human gait (Tong and Granat (1999)), but their immobility limits their use to in-lab data collections. Goniometers have been used as a conventional portable measurement tool for knee angle (Frosio et al. (2009); Lukowicz et al. (2004)), but there are issues of accuracy and wearability.

More recently, inertial BSNs have been developed for continuous, accurate, wearable motion capture (Gouwanda and Senanayake (2008)). For example, the TEMPO 3.1 system provides six-degrees-of-freedom motion capture on each node in the form factor of a wristwatch (Barth et al. (2009)). In this paper, the TEMPO 3.1 system, shown in Figure 1 mounted on a healthy human subject, was used

to measure knee joint angle, with a Vicon® system providing a reference to characterize the error sources present in TEMPO.

2.2 Data Collection

Subjects with no orthopedic or neuromuscular impairment history were mounted with TEMPO nodes and Vicon® markers on each body segment, i.e., left thigh, left shank, right thigh and right shank, as shown in Figure 1(b). The subjects were asked to walk on a treadmill continuously at 2.0 km/h, 3.0 km/h, and 4.0 km/h for 30 s each, and then at a continuous ramp-up and ramp-down between 0.0 km/h and 4.0 km/h for 60 s. Data were taken from the Vicon® and TEMPO systems simultaneously, both sampled at 120 Hz, with a predefined synchronization procedure. All the computation is performed offline, including event-based synchronization achieved by post-processing, calibration, and knee joint angle calculation.

To compute the joint angle correctly, the orientation of sensitive acceleration axes and gyroscope planes relative to the limb must be noted when instrumenting the subject. In this case, the sagittal plane contains the information of greatest interest. Therefore, signals of the X-axis and Y-axis of the accelerometer and the Z-plane of the gyroscope were used for computation.

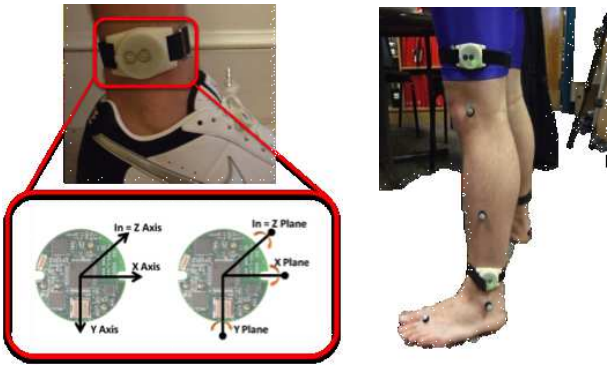

(a) (b)

Figure 1: (a) The TEMPO 3.1 node with mounting position. The TEMPO nodes are placed with the inferior direction as Y-axis positive, the posterior direction as X-axis positive, and right lateral direction as Z-axis positive. (b) The TEMPO nodes mounted on-body, along with Vicon® markers.

2.3 Joint Angle Calculation Method

Several researchers have explored ways of measuring joint angle using inertial sensors (Tong and Granat (1999); Salarian et al. (2004)). In this paper, an effective yet computationally less intensive method is applied to calculate the knee joint angle from data taken from accelerometer and gyroscope sensors. The knee angle is calculated from the accelerometer data for static postures and from the rate gyroscope data during dynamic walking.

2.3.1 Static joint angle calculation

In the static period, the accelerometers are employed to provide the inclination of each segment. The knee joint angle is obtained by comparing the tilt of the shank and the tilt of the thigh. Following the convention of the Vicon® system, we chose the ground as the reference and subtract the thigh tilt from the shank tilt. The placement of TEMPO nodes is shown in Figure 2.

$$\varphi_{segment} = \arctan\left(\frac{A_x}{\sqrt{A_y^2 + A_z^2}}\right) \tag{1}$$

In Equation (1) (Tuck and Tempe (2007)), A_x, A_y, A_z are the linear accelerations obtained from the accelerometer signals with respect to each axis, and $\varphi_{segment}$ (i.e. φ_{shank} or φ_{thigh}) is defined as the angle of the X-axis relative to ground. The knee joint angle can be found as:

$$\varphi_{knee} = \varphi_{shank} - \varphi_{thigh} \tag{2}$$

The absolute joint angle is the supplement of the angle obtained by Equation (2).

2.3.2 Dynamic joint angle calculation

We obtain dynamic gait period angles by integrating the discrete angular velocity value measured from the rate gyroscope sensors:

$$\varphi[n] = \varphi[n-1] + \frac{\triangle}{2} \times (\omega[n-1] + \omega[n]) \tag{3}$$

In Equation (3) (Salarian et al. (2004)), is the angular velocity obtained from the rate gyroscope signal, $\triangle$ is the sampling period (1/120 s in this case) and φ is the dynamic angle of each segment with respect to ground. The initial value of the dynamic angle is obtained from the static posture in every experiment session providing the initial orientation for the gyroscope. The knee joint angle is calculated by subtracting the integrated thigh angle from the integrated shank angle, as shown in Equation (2).

However, this method is subject to error accumulation due to the integration drift caused by the unpredictable gyroscope bias. We apply a high-pass filter to eliminate the drift (Barth et al. (2009)). In this paper, a 3rd order Butterworth high-pass filter with a cut-off frequency of 0.3 Hz is applied. To avoid phase-distortion caused by filtering, the filter is applied twice, forward and backward, to achieve zero-phase distortion Salarian et al. (2004). Section 5 demonstrates the effect of drift when such a filter is not applied.

A high-pass filter inevitably removes the DC signal. To compensate for this, the knee joint angle obtained from Vicon® is normalized by applying the same high pass filter.

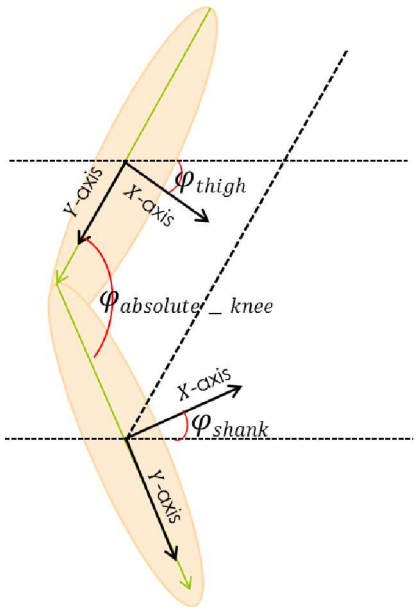

Figure 2: Accelerometer placement and knee joint angle.

3 Synchronization

BSN applications employing data fusion across multiple sensor nodes can suffer significant error if not properly time-synchronized. Computations combining non-stationary data sample-by-sample from various nodes will, for a given time lag among nodes, incur error related to the rate of change in the signals. For example, a joint angle computed from two limb segment angles will combine segment angles taken at different times and different postures; the severity of this difference is a function of the time lag between signals and the speed of the limb motion. This section details three methods for synchronization – including the time transmission synchronization used in TEMPO 3.1 – and evaluates the impact of errors when synchronization is not performed or is done so with low resolution.

3.1 Synchronization Methods

3.1.1 Network-based synchronization

Achieving time synchronization is a matter of both reconciling the time offset between nodes at a given time instant, as well as accounting for subsequent clock drift due to slight variations in clock frequency among nodes (Sundararaman et al. (2005)). Some form of message passing can correct the time offset, but errors can result from various uncertain delays as follows: the delay between message creation and arrival at the MAC layer (send time), the MAC layer delay until transmission (access time), the over-the-air transmission delay (propagation time), and the delay to receive the entirety of the message (receive time) (Sivrikaya and Yener (2004)).

Numerous synchronization methods have been proposed in the wireless sensor network (WSN) community. Reference Broadcast Synchronization (RBS) eliminates error due to send time and access time by broadcasting a message from one master node to all neighbors at once, which then compare receipt times. The Timing-synch Protocol for Sensor Networks (TPSN) and Flooding Time Synchronization Protocol (FTSP) minimize delay errors by timestamping messages at the MAC layer, and they are also designed to scale with multi-hop networks, with FTSP being more robust to topology changes (Sivrikaya and Yener (2004); Maróti et al. (2004)). For single-hop networks, these methods all offer s-order precision.

A number of other methods are surveyed in (Sundararaman et al. (2005)), which identifies some criteria for selection of an appropriate synchronization method, including energy requirements, network size, topology variability, and necessary synchronization precision. Yet, for a small, one-hop network BSN streaming data to a single aggregator at high data rates, the requirements may often be less stringent than for WSNs, and so the best method may simply be that which is already implemented or most easily implemented on the chosen platform.

3.1.2 Sensor event-based synchronization

The above methods, however, depend on message broadcast support or access to MAC-layer timing information, but these may not always be available. For instance, the TEMPO system incorporates a commodity RFCOMM-enabled Bluetooth radio, such as could be used to communicate with recent Android-based smartphones, which support only basic RFCOMM Bluetooth communication.

One solution is to instead synchronize the aggregated data based on intentionally generated sensor events. The BSN user performs some synchronization action that applies stimuli simultaneously to multiple sensors. An operator can manually note the times of the sensor events during post-processing. (Bannach et al. (2009)) describes the use of spotting algorithms for automatic detection of these events in multimodal sensor environments, and advocates repeating the synchronization action multiple times to avoid errors from false detections.

A simpler approach can suffice for synchronizing sensor streams recorded by the same type of sensor. If the time window of the synchronization action is recorded by an operator via aggregator software, offline processing can automatically examine this window to determine the lag between streams. The time lag (as a number of samples) between the two streams is that which maximizes the cross-correlation between them. Since the measurement and adjustment of time lag can be performed offline, this approach requires no firmware modifications to the BSN platform, and thus proved useful and sufficient for synchronizing TEMPO nodes in this study.

Event-based synchronization can be useful not only for synchronization within a BSN, but between BSNs that are not necessarily programmed to interoperate. Furthermore, it can be used to synchronize against a non-BSN system, such as an optical motion capture system for ground-truth

validation of an inertial BSN experiment, but manual spotting of the events may be necessary. For example, in this study, synchronization between the TEMPO and Vicon® systems was achieved by striking a TEMPO node against a Vicon® system force plate. Similarly, video recordings of experiments can be synchronized to BSN data by selecting the video frame during which a synchronization action occurred.

3.1.3 Time transmission-based synchronization

An alternative synchronization approach utilizes the time transmission protocol (TTP) commonly used in distributed systems (Arvind (2002)) and which has also been applied to wireless sensor networks (Sundararaman et al. (2005)). This method allows a microcontroller to control synchronization while bypassing the inaccessible radio MAC layer in some commercial radios. In TEMPO 3.1, a star topology with a data aggregator in the center is used, i.e., communication only occurs between the aggregator and nodes, thus the TTP scheme aims to discover a relationship between the aggregator clock and each sensor node clock. When synchronizing, first clock information is exchanged between the data aggregator and the sensor nodes. Then the sensor nodes send a series of timestamps, each at time T of the nodes clock. The aggregator receives such timestamp at time R of the aggregators clock, with an unknown delay d, due to the transmission delay over the radio (Arvind (2002)). The aggregator estimates the nodes clock based on Equation (4) (Arvind (2002)):

$$T_{node} = R_{A_n} - \overline{R_{A_n}}(n) + \overline{T_{node}}(n) + \overline{d} \qquad (4)$$

where $\overline{R_A}$ is the average of all the aggregator timestamps of received messages, R_{A_n} is the last aggregator timestamp, T_{node} is the average of the node timestamp for transmitting a message, and $\overline{d}$ is the average delay.

This equation assumes that the clocks of both peers operate at the same basic frequency. However, in our case, this is not true – specifically, the node and aggregator maintain software timers operating at 120 Hz and 1 kHz, respectively – and thus we must normalize the aggregator's timestamps to those of the node by multiplying by a ratio of their basic frequencies, leading to equation (5).

$$T_{node} = \frac{f_{node}}{f_A} R_{A_n} - \frac{f_{node}}{f_A}\overline{R_A}(n) + \overline{T_{node}}(n) + \frac{f_{node}}{f_a}\overline{d} \quad (5)$$

Since the clock rate of each sensor node is assumed to be accurate in this paper, only the time lag (i.e., asynchronization) between multiple nodes is considered. Once these clock relationships are established, the nodes begin taking data and transmit the timestamps corresponding to when they started collecting data. The aggregator can therefore synchronize the multiple data streams based on the clock information and timestamps.

Ideally, TTP synchronization would provide the maximum cross-correlation at zero. However, in reality, a deviation between the two synchronization methods can be as high as a few samples or tens of milliseconds. Compared to event-based synchronization, TTP synchronization eliminates a pre-defined synchronization procedure and post processing. With the cost of a small amount of delay in the beginning of data collection, TTP synchronization enables the on-body data collection to be sped up, slowed down, and even stopped and restarted without requiring the user to perform any re-synchronization action.

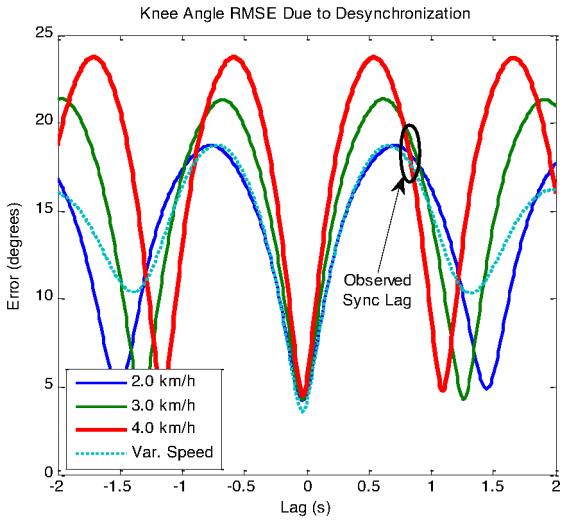

Figure 3: Knee angle RMSE for simulated -2s to +2s lag.

3.2 Joint Angle Error Due to Time Lag

The joint angle calculation in Equation (2) involves a subtraction between angles derived from separate nodes on a sample-by-sample basis. For a time lag of m samples between the thigh and shank nodes, segment angles occurring m seconds apart are compared as though they occurred simultaneously, adding error to the calculation.

The potential desynchronization error was extrapolated from the experimental gait data described in Section 2.2 over a range of time lags between the shank and thigh nodes, from -2s to +2s in $1/\triangle$ s increments. The resulting RMSE depends on the gait speed since, for a given lag, the shank and thigh are farther apart in the gait cycle at faster gait speeds. Also, the RMSE is periodic with a period equal to the gait period (i.e., the nodes are effectively in phase if they are separated in time by an integer number of gait cycles that are somewhat symmetric cycle-to-cycle).

The knee angle RMSE is shown in Figure 3. The RMSE is minimized at zero lag, where there remains a roughly 4° error, to be addressed in subsequent sections. The highlighted data points correspond to the actual lag observed in this trial between the shank and thigh nodes when synchronization was not applied. This rather large lag results in an increase of about 17° in the RMSE relative to the synchronized case. A medium-speed gait reaches a 5° increase in RMSE around a 100 ms lag, but a lag around 15 ms can be tolerated to within 1°. Certainly any synchronization method guaranteeing 1 ms precision or better would be sufficient for this application. Other applications

may require greater or lesser synchronization precision.

4 Sensor Calibration

Accelerometers and rate gyroscopes used in inertial BSN platforms are typically assumed to follow a linear model. The relationship between the sensed quantity (M), and the output voltage (V), is described by Equation (6), which contains two key parameters: the sensitivity (S) and the offset (O).

$$M = \frac{(V - O)}{S} \tag{6}$$

The sensitivity is the ratio of voltage change to change in the physical quantity, and the offset is the output voltage when no motion (or gravitational field, in the case of accelerometers) is applied to the sensor. These parameter values can be found in the sensor datasheets, but in practice they will deviate from the expected value.

Sources of sensor error include manufacturing variations and environmental conditions, such as temperature, meaning that sensitivity and offset will vary both across different sensors at a given time, or within a single sensor at various times. Datasheets and white papers from manufacturers additionally list other possible error sources, such as nonlinearity, non-orthogonality between axes, and cross-axis sensitivity. Finally, variations in chip mounting on a PCB or mounting of the PCB in the node packaging can place the sensing axes slightly out of the assumed frame of reference.

4.1 Methods

It is impractical to individually compensate for these sources of error, and so some form of calibration is employed to holistically minimize their effect. The sensor response is checked against a known reference point (such as the gravitational field or a turntable) in order to calculate the actual sensitivity and offset by linear mapping or Newtons method (Frosio et al. (2009); Lukowicz et al. (2004); Borenstein et al. (2009); Krohn et al. (2005)). This section evaluates three different calibration techniques both on- and off-body.

4.1.1 Linear mapping technique

The simplest calibration technique is the linear mapping of two points measured with respect to gravity into the linear function of Equation (6). The sensitivity (S) and offset (O) are calculated from these reference points according to Equation (7).

$$\begin{cases} S = \frac{V_{max} - V_{min}}{2g},\ O = \frac{V_{max} + V_{min}}{2}\ (Accelerometer) \\ S = \frac{V_{max} - V_{min}}{400°/s},\ O = \frac{V_{max} + V_{min}}{2}\ (Gyroscope) \end{cases} \tag{7}$$

For accelerometers, each axis of sensor is exposed to 1g and -1g by placing it parallel with gravity. Similarly, rate gyroscope sensors can be placed on a turntable and subjected to the available rotational rates, typically 33 RPM and 45 RPM.

4.1.2 Mathematical estimation technique

The mathematical estimation technique is based on the principle that the sum of vector magnitude of 3-axes accelerations is 1g when the accelerometer is stationary. This technique only applies for accelerometers. This principle is described by Equation (8)

$$\sqrt{A_x^2 + A_y^2 + A_z^2} = 1g \tag{8}$$

The three-axis accelerometer sensor is subjected to the gravitational field in six arbitrary orientations (rather than with each axis subsequently placed parallel with gravity). Each set of voltage measurements, V_x,V_y,V_z, gives rise to an equation of the form given by Equation (7), where S_i and O_i are the sensitivity and offset, respectively, of axis i.

$$F(S_x, S_y, S_z, O_x, O_y, O_z) = \sqrt{(\frac{V_x - O_x}{S_x})^2 + (\frac{V_y - O_y}{S_y})^2 + (\frac{V_z - O_z}{S_z})^2} - 1 = 0 \tag{9}$$

The resulting system of six equations can be solved for the sensitivities and offsets by a mathematical iterative estimation, such as the Newton-Raphson method. An arguable advantage of this technique is that it does not require a perfectly level surface for calibration, but it does require an initial computational complexity due to the iterative estimation (Lukowicz et al. (2004)).

4.1.3 Piecewise mapping technique

The previous techniques assume a linear sensor model, but a piecewise linear equation may better fit the nonlinearities in the sensor response. This procedure requires profiling the sensor against more than two known reference points and mapping the readings into a piecewise linear function. For an n-point linear function, the nth sensitivity and offset are given as follows:

$$\begin{cases} S(n) = \frac{V_n - V_{n-1}}{(cos\theta_n - cos\theta_{n-1})g},\ O = \frac{V_n + V_1}{2}\ (Accelerometer) \\ S(n) = \frac{V_n - V_{n-1}}{(\omega_n - \omega_{n-1})°/s},\ O = \frac{V_n + V_1}{2}\ (Gyroscope) \end{cases} \tag{10}$$

with n being the number of required measurement points. The most convenient and commonly-used choice of n is 3 data points, such as 0°, 90°, and 180°. However, increasing the number of data points increases the conversion accuracy, as detailed in the following section.

Table 1: Accuracy analysis of 1-axis calibrated accelerometer.

Calibration Techniques	**RMSE**	**Mean of Angle Error (deg)**
Datasheet Conversion	22.75	20.95
Newton	1.63	0.26
Linear	1.53	0.24
Piecewise ($n = 3$)	1.51	0.22
Piecewise ($n = 5$)	0.78	0.20
Piecewise ($n = 7$)	0.70	0.15

4.2 Calibration Experiment

4.2.1 Off-body analysis

In order to accurately test and measure angles obtained by accelerometer data, a digital inclinometer instrument with $\pm 0.5°$ error was used. A typical turntable with two constant speed settings, 33 RPM ($200°/s$) and 45 RPM ($270°/s$), were used for gyroscope calibration and verification. Figure 4 shows the experiment setup of accelerometer and gyroscope for calibration and measurement. Note, the TEMPO node is placed in a custom bracket used to precisely place it in the desired frame of reference.

(a) Inclinometer (b) Turntable

Figure 4: Calibration and measurement instrument.

Table 1 shows a comparison among 4 calibration methods for the accelerometer, including piecewise mapping with n = 3, 5, and 7. Datasheet conversion refers to the baseline case using the sensitivity and the offset listed in the sensor datasheet. In order to verify the output, the measurement was performed at 10 increments from 0° to 180° on the inclinometer. Piecewise calibration results in the lowest RMSE, with more data points providing higher accuracy, although the additional efforts to obtain a high n must be balanced against the accuracy improvements.

To verify the accuracy of the three gyroscope calibration methods, the calibration results from two different speeds, respectively, are verified by the other three speeds, as shown in Figure 5. Figure 5 shows that there is no significant difference between the calibration reference speed, as in our case, $270°/s$ and $200°/s$. Also the 3-points piecewise calibration and linear calibration have almost the same linear response to ADC values, and verification speed points fall on the piecewise line and linear line, indicating a good calibration result, while there are as high as $45°/s$ error of datasheet calibration method.

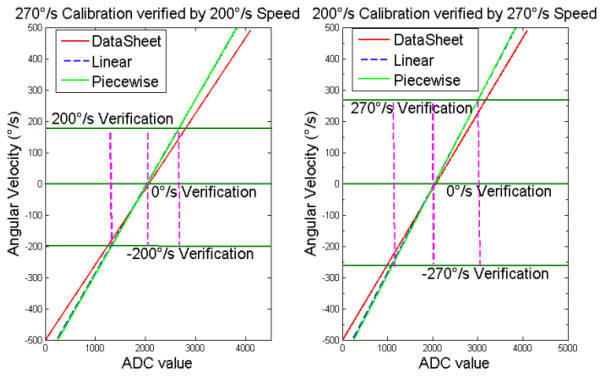

Figure 5: Gyroscope calibration and speed verification.

Table 2: Static knee joint angle between Vicon® and TEMPO.

Vicon®	**TEMPO Angle Error** (deg)			
	Datasheet Conv.	**Linear Calib.**	**Newton Raphson**	**Piecewise Calib.** ($n = 3$)
0.66	12.37	8.22	6.16	9.73
54.76	25.32	15.70	18.14	16.88
65.21	24.24	15.36	17.51	16.21
83.32	25.01	17.60	19.05	17.8
104.09	33.73	31.13	32.07	30.84

Table 3: Dynamic knee joint angle RMSE (in degrees) comparing Vicon® and TEMPO.

Gait Speed (km/h)	**Measurement Error (RMSE)**		
	Datasheet	**Linear**	**Piecewise** ($m = 3$)
2	8.72	2.75	3.59
3	9.51	3.03	3.88
4	9.87	3.15	4.01
Varying Speed	8.96	2.86	3.67

4.2.2 On-body analysis

TEMPO nodes were mounted on human subjects as stated in Section 2, for the purpose of verifying the calibration in the context of knee joint angle measurement. Of the above-described calibration techniques were tested for static and dynamic knee joint angle measurement and compared against results from the Vicon® system. All data was synchronized using the technique stated in Section 3.1.2.

Table 2 shows the results of static knee joint angle measurement using accelerometers corresponding to different postures. Although error is minimized with the best calibration method (piecewise) as shown in the off-body analysis, the errors are tremendously increased when put on-body, which may even disguise the impact of calibration.

The results of the dynamic joint knee angle analysis are shown in Table 3. The measurements were taken at dif-

ferent gait speeds: constant speeds of $2km/h$, $3km/h$, and $4km/h$, as well as a varying-speed trial. While calibration still results in an improved RMSE compared to using only datasheet-supplied values, there is a large error compared to the off-body tests, which may be attributed to mounting error, as discussed in the next section.

5 Integration Drift

Integration drift is inherent in any inertial sensor system and occurs when converting from acceleration to velocity (or again to position displacement) or from rotational rate to angular displacement. Here we focus on the latter, as discrete integration is applied to the gyroscope data in Equation (3). It is well-known that drift occurs as a function of time and acts as a DC offset in the gyroscope due to intrinsic sensor errors such as random noise and bias that are accumulated with time during integration. As discussed in Section 2.3.2, this DC offset can be effectively removed with a high-pass filter, as was done for the results in the other sections in this paper. However, this section characterizes integration drift and demonstrates its potential impact on the knee joint angle application if not properly addressed.

To do so, a sensor node was placed on the turntable from 1 full rotation to 10 rotations with an increment of 1 rotation, and for 15, 20, and 30 rotations, with a time span of 1.8 s at $200°/s$ and 1.33s at $270°/s$ for each rotation. The experiment for each rotation number was repeated three times to reduce the uncertainty and observation error, with a standard deviation no larger than 5°. The experiments were performed in both the positive and negative directions. The integration error is computed as the deviation of the integrated angles using the raw angular velocity (calibrated using the above piecewise method) from the reference angles (i.e., number of rotations $\times 360°$). The results are shown in Figure 6.

As expected, the integration error significantly follows a linear relationship over time and does not depend heavily on the speed of rotation. When integrating, the positive angular velocity drifts almost symmetrically as the negative angular velocity.

To demonstrate the impact of this drift on knee angle calculations, the shank angular velocity and thigh angular velocity were collected from human subjects without the low pass filter described in Section 2.3.2. As shown in Figure 7, the shank angle drifts in the negative direction, and the thigh angle drifts in the positive direction. In both cases, the gyroscopes are seeing rotation in both directions, by the shank spends a larger percentage of time rotating in the negative direction, resulting in an overall negative drift, and vice versa for the thigh. It is clear in Figure 7 that such drift rapidly results in unacceptable errors for knee joint angle calculation.

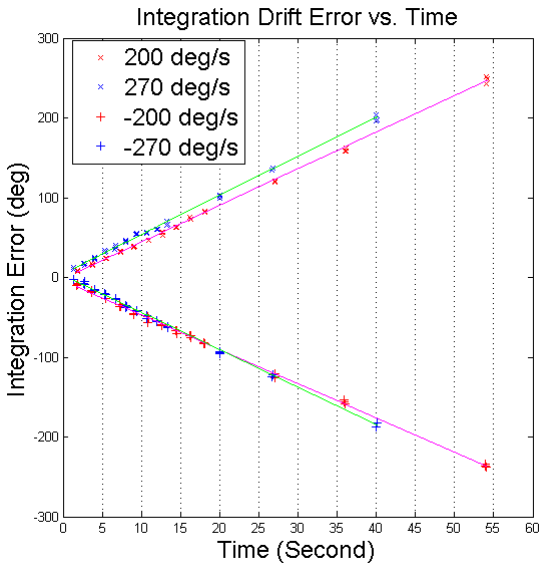

Figure 6: Gyroscope integration drift.

6 Mounting Calibration

Mounting error has emerged as the dominant error source in this application, resulting in a large knee angle error even after other errors have been minimized. In this section, we investigate various mounting errors in inertial BSNs affecting both accelerometers and rate gyroscopes and discuss correction methods for different mounting errors.

6.1 Static Mounting Error Compensation

While the calculation of knee angle during static periods (i.e. no movement) should be easily derived from the analysis in Section 2.3.1, mounting error introduces significant inaccuracies, including errors up to 30.8 degrees (see Table 2). The tilt detection mechanism of accelerometers brings up a trade-off in static angle measurement. On one hand, the accelerometers are sensitive to detect the tilt when precisely positioned. On the other hand, this sensitivity makes them prone to noisy tilt introduced by body shape instead of segment inclination.

We identify the mounting errors affecting accelerometers as following:

1. When the motion sensor is mounted on a human body, the axes of acceleration can be shifted and rotated from the assumed orientations due to the nodes becoming mis-positioned on the body or rotated via muscle flexion and extension. Therefore, calculating the angle with respect to the assumed coordinate results in an error. In particular, a slight rotation in the Z-plane away from the expected mounting adds error to the angle measured by the two major sensing axes (X and Y).

2. The specific reference points for knee joint angle cal-

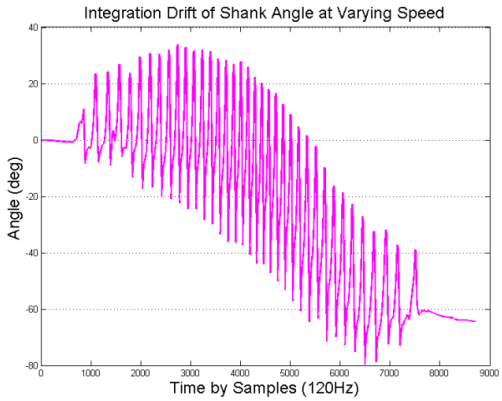

(a)

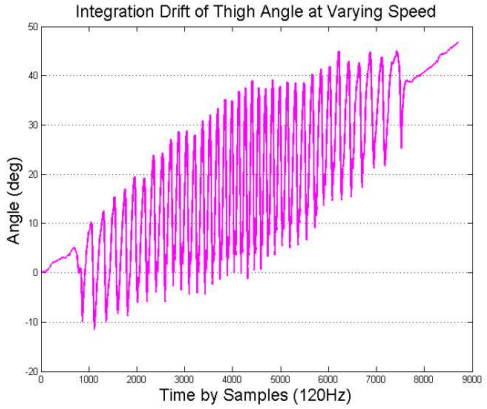

(b)

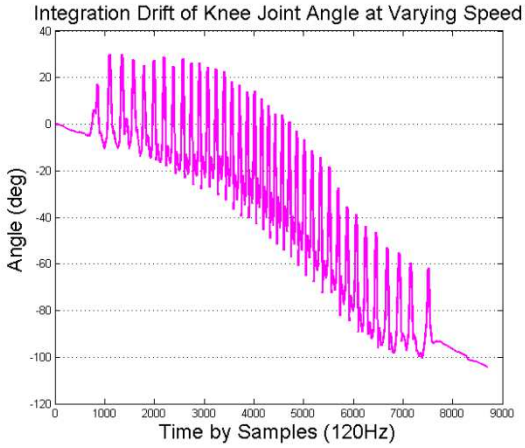

(c)

Figure 7: Integration drift of shank angle, thigh angle, and resulting knee angle at varying gait speeds.

culation are different for Vicon® and TEMPO. The Vicon® system captures the anatomy of the human subjects and produces knee joint angle as the angle between the femur and tibia bones, while TEMPO system are mounted on skin where the angle is similar but not equivalent to the bone-to-bone knee angle, which leaves a discrepancy with the angle measured by reference system.

Table 4: Improved accuracy after cyclic error compensation

Gait Speed	**Without Error Compensation**		**With Error Compensation**	
	Coefficient	**RMSE**	**Coefficient**	**RMSE**
2km/h	0.9935	2.70	0.9950	1.65
3km/h	0.9930	3.00	0.9969	1.40
4km/h	0.9919	3.14	0.9962	1.61
Varying Speed	0.9911	2.79	0.9959	1.51

The inaccuracies seen in Table 2 include both of these error sources. A simple approach to compensating for these errors is to use an initial reference posture to determine an offset ma gnitude that is then used to adjust the other calculated angles. By doing this, we improved the accuracy with an average residual error of 10.7 degrees.

6.2 Dynamic Mounting Error Compensation

The dynamic knee joint angle retrieved from the rate gyroscope sensed angular velocity is affected by mounting error as well. Comparing with mounting error affecting accelerometer data, we found:

1. Data from the z-plane gyroscope does not change if the gyroscope is rotated on the z-plane, and the mounting orientation does not affect the gyroscope data as badly as the accelerometer data.

2. The gyroscope-recorded knee joint angle signal is attenuated compared to the reference signal due to the anatomy capture difference.

3. With a careful inspection of the human gait, it is noticeable that during walking, though most of the swing motion is located on sagittal plane, subtle rotations happen on other planes, too (Ross Bogey (2009)). Therefore, using only the z-plane gyroscope signal, the limb rotation and the final knee joint swing range will be attenuated as shown in Figure 8 (comparing TEMPO to Vicon®).

Because of the complexity of the gait motion, further study and more refined modeling are required to compensate for mounting error. For example, a possible solution for error compensation in periodical gait signals leverages the fact that the error waveforms (i.e. Vicon® vs. TEMPO) are also periodic with the gait cycle, as plotted in Figure 8 (Error before Compensation). It is therefore possible to characterize the error for a number of gait cycles and then apply a compensating signal to all subsequent cycles. In this paper, we average the error taken from 25 cycles within each speed session and add this averaged cyclic error to the original knee joint angle of each gait cycle. It can be seen in Figure 8 that the resulting Compensated Joint Anglenearly matches Vicon®.

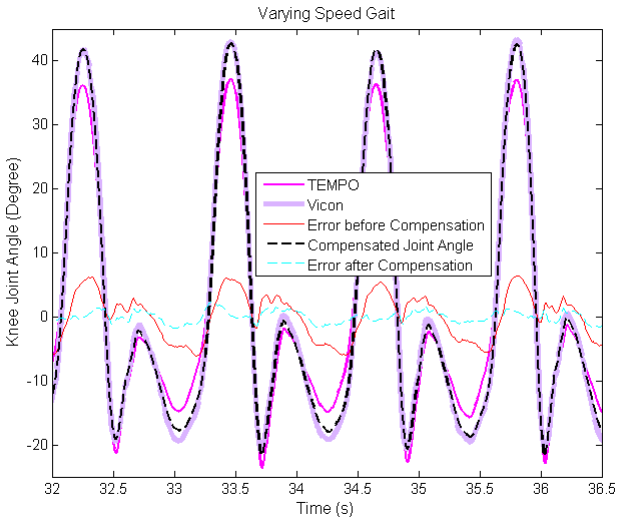

Figure 8: Cyclic error compensation method.

Table 4 shows that after applying the cyclic error compensation, the average correlation between the TEMPO measured knee joint angle and

Vicon® has increased from 0.9924 to 0.9960, and the average RMSE has reduced from 2.91 degrees to 1.54 degrees. Comparing with the results achieved in (Barth et al. (2009)), which gives a correlation of 0.98 and RMSE of 3.98 degrees, an improvement thanks to the error characterization has been shown.

This cyclic error compensation method must be validated against different subjects and speeds. It may also conceal the possible controllable sources of errors. Therefore, it should be only used after all of the other error sources in the system have been minimized.

7 Conclusion

While the synchronization, calibration, and drift error sources discussed in this paper are inherent in any inertial BSN, it is necessary to characterize the fidelity impact of such errors on the target application. While such analysis is application-specific (and must therefore be repeated for each application), it is essential for achieving required application fidelity with emerging BSN platforms.

In this paper, time synchronization, sensor calibration, integration drift, and mounting calibration error sources were characterized for knee joint angle measurement (common in physical rehabilitation and gait research) using TEMPO 3.1, a multi-node inertial BSN. Vicon®, an industrial optical motion capture system, was used for quantifying error and evaluating the effectiveness of various methods for minimizing error, including the time transmission synchronization approach used in TEMPO 3.1. The error sources were determined to have significantly different effects on application fidelity. Mounting calibration proved to be the biggest challenge, but compensation methods were explored that provided accuracy up to an RMSE of 1.5 degrees during walking, which is within the range of error in the optical motion capture system.

Future work includes both application-specific efforts to maximize the fidelity of motion analysis using inertial BSNs and the development of a generic framework for connecting low-level error sources to ultimate application fidelity.

8 Acknowledgements

This paper is an extended version of one that was presented at *BodyNets 2010* (Chen et al. (2010)), The authors would like to thank Dr. Bradford Bennett and the whole Motion Analysis & Motor Performance Laboratory team at the University of Virginia Children's Hospital for their assistance. This work is supported in part by the University of Virginia Biomedical Innovation Fund and the National Science Foundation under grant Nos. CBET-0756645 and CBET-1034071.

REFERENCES

Arvind, K. (2002). Probabilistic clock synchronization in distributed systems. *IEEE Transactions on Parallel and Distributed Systems*, 5(5):474–487.

Bannach, D., Amft, O., and Lukowicz, P. (2009). Automatic event-based synchronization of multimodal data streams from wearable and ambient sensors. *European Conference on Smart Sensing and Context*, pages 135–148.

Barth, A., Hanson, M., Powell, H., and Lach, J. (2009). Tempo 3.1: a body area sensor network platform for continuous movement assessment. In *International Workshop on Wearable and Implantable Body Sensor Networks*, pages 71–76.

Borenstein, J., Ojeda, L., and Kwanmuang, S. (2009). Heuristic reduction of gyro drift in IMU-based personnel tracking systems. In *Proceedings of the SPIE*.

Chen, S., Brantley, J. S., Kim, T., and Lach, J. (2010). Characterizing and minimizing synchronization and calibration errors in inertial body sensor networks. In *International Conference on Body Area Networks*.

Frosio, I., Pedersini, F., and Borghese, N. (2009). Autocalibration of MEMS accelerometers. *IEEE Transactions on Instrumentation and Measurement*, 58(6):2034–2041.

Gouwanda, D. and Senanayake, S. (2008). Emerging trends of body-mounted sensors in sports and human gait analysis. In *International Conference on Biomedical Engineering*, pages 715–718.

Krohn, A., Beigl, M., Decker, C., Kochendörfer, U., Robinson, P., and Zimmer, T. (2005). Inexpensive and automatic calibration for acceleration sensors. *Ubiquitous Computing Systems*, pages 245–258.

Lukowicz, P., Junker, H., and Tröster, G. (2004). Automatic calibration of body worn acceleration sensors. *Pervasive Computing*, pages 176–181.

Maróti, M., Kusy, B., Simon, G., and Lédeczi, Á. (2004). The flooding time synchronization protocol. In *International conference on Embedded networked sensor systems*, pages 39–49.

Ross Bogey, D. (2009). Gait analysis http://emedicine.medscape.com/article/320160-overview.

Salarian, A., Russmann, H., Vingerhoets, F., Dehollain, C., Blanc, Y., Burkhard, P., and Aminian, K. (2004). Gait assessment in Parkinson's disease: toward an ambulatory system for long-term monitoring. *IEEE Transactions on Biomedical Engineering*, 51(8):1434–1443.

Sivrikaya, F. and Yener, B. (2004). Time synchronization in sensor networks: a survey. *IEEE Network*, 18(4):45–50.

Sundararaman, B., Buy, U., and Kshemkalyani, A. (2005). Clock synchronization for wireless sensor networks: a survey. *Ad Hoc Networks*, 3(3):281–323.

Tong, K. and Granat, M. (1999). A practical gait analysis system using gyroscopes. *Medical engineering and physics*, 21(2):87–94.

Tuck, K. and Tempe, A. (2007). Tilt sensing using linear accelerometers. *Freescale Semiconductors Inc. application note AN3461*.